11370 *Inorg. Chem.* **2010**, *49*, 11370–11377
DOI: 10.1021/ic101177d

Inorganic Chemistry
Article

Polytypism, Disorder, and Anion Exchange Properties of Divalent Ion (Zn, Co) Containing Bayerite-Derived Layered Double Hydroxides

Sylvia Britto and P. Vishnu Kamath*

Department of Chemistry, Central College, Bangalore University, Bangalore 560 001, India

Received June 11, 2010

Incorporation of Zn^{2+} into bayerite results in the formation of a cation-ordered layered double hydroxide (LDH) of monoclinic symmetry in which about half the vacancies of $Al(OH)_3$ are occupied by Zn^{2+} giving rise to positively charged layers. Charge compensation takes place by the incorporation of sulfate ions in the interlayer region. Structure refinement reveals that the adjacent layers in the crystal are related by a 2_1 axis (we call it $2M_1$ polytype) with sulfate coordinating in the D_{2d} symmetry in the interlayer region. Another polytype in which adjacent layers are related by a 2-fold axis ($2M_2$ polytype) can also be envisaged. Faulted crystals arising from intergrowths of the $2M_2$ polytype within the $2M_1$ structure were also obtained. These bayerite-based LDHs have a distinctly different interlayer chemistry when compared to the better known brucite-based LDHs, in that they have a strong affinity for tetrahedral ions such as SO_4^{2-}, CrO_4^{2-}, and MoO_4^{2-} and a poor affinity for CO_3^{2-} ions. These observations have implications for the use of LDHs in applications related to chromate sorption.

Introduction

Mineral brucite, $Mg(OH)_2$,[1] has industrial importance as a precursor to the solid base catalyst MgO.[2] The surface basicity of $Mg(OH)_2$ may be tuned by the partial substitution of Mg^{2+} ions by trivalent ions, resulting in the formation of the well-known class of materials known as the layered double hydroxides (LDHs).[3] These materials are important precursors to high surface area solid base catalysts. The LDHs themselves exhibit enhanced base catalytic activity,[4] sorption,[5] and anion exchange properties.[6]

The more acidic hydroxide, $Al(OH)_3$,[7] is an important precursor to the synthesis of the aluminas which are acid catalysts and used as catalyst supports and adsorbents.[8,9] $Al(OH)_3$ is isotypic with $Mg(OH)_2$ and comprises an approximate close packing of hydroxyl ions in which two-thirds of the octahedral sites in alternative layers are occupied by Al^{3+} to yield charge-neutral layers having the composition $[Al_2\square(OH)_6]$ ($\square$: cation vacancy).

$Al(OH)_3$, like $Mg(OH)_2$, lacks any interlayer chemistry and thereby its applications are limited. The cation vacancies in $Al(OH)_3$ are ordered in such a manner as to minimize cation−cation repulsions. Vacancy ordering causes a reduction in crystal symmetry to monoclinic symmetry compared to the hexagonal symmetry of $Mg(OH)_2$. As in the brucite-based LDHs, $Al(OH)_3$ too can be imparted with a surface basic character and interlayer chemistry by generating a positive charge on the metal hydroxide layer. This can in principle, be achieved by "imbibing"[10] an additional cation, M^{n+}, in the vacancies, to generate positively charged metal hydroxide layers having the composition $[(M^{n+})_{1/n}\square_{1-1/n}Al_2(OH)_6]^+$. However, the only successful synthesis reported to date is the LDH of Li with Al, having the limiting composition $[LiAl_2(OH)_6](A^{n-})_{1/n}\cdot mH_2O$ (A = Cl, Br, SO_4, CO_3, NO_3).[11] We refer to this as the I−III LDH.

The possibility of generating $Al(OH)_3$-based LDHs containing divalent cations, with the idealized compositions $[(M^{II})_{0.5}\square_{0.5}Al_2(OH)_6]^+$ was proposed.[12,13] Fogg and coworkers[14] reported the synthesis of LDHs with similar compositions without clear evidence or results of structure refinements. The chief difficulty in realizing compounds with such compositions lies in the high cation−cation repulsions that cannot be adequately screened by the hydroxyl ion sublattice. When for instance, all the octahedral vacancies are occupied by Al^{3+} ions, some of the OH^- ions are transformed to O^{2-}, as in

*To whom correspondence should be addressed. E-mail: vishnukamath8@hotmail.com.

(1) Oswald, H. R.; Asper, R. *Preparation and Crystal Growth of Materials with Layered Structures*, Dreidel Publishing Company: Dordrecht, The Netherlands, 1977.
(2) Liang, S. H. C.; Gay, I. D. *J. Catal.* **1986**, *101*, 293.
(3) Cavani, F.; Trifiro, F.; Vaccari, A. *Catal. Today* **1991**, *11*, 173.
(4) Reichle, W. T. *Solid State Ionics* **1986**, *22*, 135.
(5) Ookkubo, A.; Ooi, K.; Hayashi, H. *Langmuir* **1993**, *9*, 1418.
(6) Newman, S. P.; Jones, W. *New J. Chem.* **1998**, 105.
(7) Megaw, H. D. *Z. Kristallogr.* **1934**, *87*, 185.
(8) Tanabe, K.; Holderich, W. F. *Appl Catal., A* **1999**, *181*, 399.
(9) Grange, P. *Catal. Rev. Sci. Eng.* **1980**, *21*, 135.
(10) Poeppelmeier, K. R.; Hwu., S.-J. *Inorg. Chem.* **1987**, *26*, 3297.
(11) Serna, C. J.; Rendon, J. L.; Iglesias, J. E. *Clays Clay Miner.* **1982**, *30*, 180.
(12) Isupov, V. P. *J. Struct. Chem.* **1999**, *40*, 672.
(13) Rajamathi, M.; Thomas, G. S.; Kamath, P. V. *Proc. Indian Acad. Sci (Chem Sci.)* **2001**, *113*, 671.
(14) Fogg, A. M.; Williams, G. R.; Chester, R.; O'Hare, D. *J. Mater. Chem.* **2004**, *14*, 2369.

 Published on Web 11/15/2010

AlO(OH), to screen the cation−cation repulsions. Besides, the metal oxide-hydroxide layer is puckered in AlO(OH). There is therefore immense scientific interest in the synthesis of Al-$(OH)_3$-based LDHs containing different metal ions and in the investigation of their structures. Further $Al(OH)_3$ itself crystallizes in a number of polymorphic modifications of which the most common are gibbsite[7] and bayerite.[15] The main difference between the two polymorphs is in the stacking sequence of the hydroxyl ions. In gibbsite the hydroxyl ions are stacked in an eclipsed manner (AB BA AB...) whereas in bayerite the stacking sequence is approximately AB AB AB...

From the point of view of applications, the Li−Al LDHs exhibit shape selective catalysis.[16−18] This selectivity has a structural basis and is thought to arise because of cation ordering.

In this paper, we report the synthesis and structure refinement of an $Al(OH)_3$ based II−III LDH containing Zn and Co. Hydrothermal treatment of bayerite in a $ZnSO_4$ solution results in a highly crystalline product whereas reaction of ZnO with $Al_2(SO_4)_3$ solution results in a compound with structural disorder. While the incidence of polytypism and stacking disorders is well understood in the hexagonal brucite-based LDHs, similar phenomena in $Al(OH)_3$-based LDHs are not described.[19] We investigate the potential for polytypism in the $Al(OH)_3$-based II−III LDHs and show that the anion exchange properties of these LDHs are distinctly different from those of the brucite-based II−III LDHs.

Experimental Section

LDH Synthesis. $Al(OH)_3$-based II−III LDHs were prepared by soaking 0.5 g of bayerite (prepared using a literature procedure)[10] in ∼2.8 M (40 mL) $ZnSO_4$ solution and hydrothermally treating the suspension in a Teflon lined autoclave (50% filling) at 150 °C for 24 h. We call this sample as ZA-1. Other compounds were similarly prepared using MSO_4 or $M(NO_3)_2$ solutions (M = Co^{2+}, Ni^{2+}). For comparison a sample, ZA-2, was prepared by soaking 1.96 g of ZnO in 20 mL of 0.75 M $Al_2(SO_4)_3$ solution and stirring the suspension at 80 °C for 24 h. All the products were washed 4−5 times with distilled water, once with isopropanol, and dried in an air oven at 65 °C.

All samples were characterized by powder X-ray diffraction (Bruker D8 Advance Diffractometer, Cu Kα radiation, λ = 1.5418 Å, reflection geometry). Data were collected at a continuous scan rate of 1° 2θ min^{-1} and a step size of 0.02° 2θ. For Rietveld refinement, data were collected over 5−100° 2θ (step size 0.02° 2θ, continuous scan rate of 10 s step^{-1}).

Rietveld refinement was carried out using the GSAS software package.[20] For the refinement, a TCH-pseudo-Voigt line shape function[21] (Profile Function 2) with eight variables was used to fit the experimental profile. A cosine Fourier series function with eight terms was used to refine the background. Bond distance restraints were imposed on Al−O (1.940 ± 0.05 Å), Zn−O (2.050 ± 0.05 Å), and S−O (1.48 ± 0.03 Å) bonds to enable stable refinement. The relative weights of these restraints were reduced as the refinement progressed with the final soft restraint weight factor being 50.

Simulations of the powder X-ray diffraction (PXRD) patterns were carried out using the program DIFFaX.[22,23] Within the DIFFaX formalism, a solid is treated as a stacking of layers of atoms and the PXRD pattern computed by integrating the diffraction intensity layer by layer. This is ideally suited for layered materials where the layers exist naturally as a consequence of anisotropic bonding. The transformation matrices required to define a monoclinic cell in DIFFaX as well as the input used for the simulation are given as Supporting Information, SI.1. and SI.2, respectively.

The LDH composition was determined by a combination of chemical and instrumental methods. Al^{3+} content was estimated gravimetrically as Al_2O_3. The divalent metal ion content was estimated by Atomic Absorption Spectroscopy (Varian AA240) and sulfate by Ion Chromatography (Metrohm Model 861 Advanced Compact ion chromatography fitted with a Metrosep A SUPP5 anion column and conductivity detector). The results are given in Table 1. The intercalated water content is determined from thermogravimetry (TGA) data (Mettler Toledo TG/SDTA Model 851^e system, 30−800 °C, heating rate 5° min^{-1}, flowing air). IR spectra were recorded using a Bruker Alpha-P FTIR spectrometer (ATR mode, 400−4000 cm^{-1}, 4 cm^{-1} resolution).

Results and Discussion

The PXRD pattern of the sample (ZA-1) obtained by hydrothermally treating bayerite in $ZnSO_4$ solution (Figure 1) is indexed to a monoclinic cell derived from the structure of the mineral nickelalumite[24] (Space group: $P2_1/n$, cell parameters: a = 10.305(3) Å, b = 8.911(2) Å, c = 17.141(2) Å, β = 95.68(2)°) (See Supporting Information, SI.3 for the list of d-spacings and their assignment). The sharp and symmetric peaks in the PXRD pattern of sample ZA-1 is characteristic of a high degree of crystallinity. We therefore first refine the structure of this compound by the Rietveld method.

We use the structure of mineral nickelalumite[24] as a model. The nickelalumite structure is closely related to that of bayerite/gibbsite and can be described as arising from the incorporation of divalent cations into half the octahedral vacancies of [Al_2□ $(OH)_6$] to give a structure having the composition [$M_{0.5}$□$_{0.5}Al_2(OH)_6$][SO_4]$_{0.5}$ (M = Ni^{2+}). While the composition of the ideal nickelalumite structure corresponds to an Al/M^{2+} ratio of 4, elemental analysis (Table 1) indicates an Al/Zn ratio of ∼3 for ZA-1. In the absence of any unitary phase of Zn, the excess Zn is expected to partially substitute for Al^{3+} yielding the layer composition [($Zn_{0.5}$□$_{0.5}$)($Al_{1.8}Zn_{0.1}$□$_{0.1}$)-$(OH)_6$]$^{0.6+}$. This kind of substitution leads to a decrease in the layer charge. The observed sulfate content matches with the layer charge, and is less than the sulfate content of the model structure. As the number of interlayer atoms is determined by the crystallographically allowed sites, the shortfall in the atom count because of sulfate deficiency is made up by the inclusion of water molecules. The nickelalumite structure of the nominal composition allows for 1.5 H_2O molecules/formula unit. The TGA data of ZA-1 indicates a higher water content of 1.8 molecules. The oxygen atoms of the additional water molecules are assigned to the same sites as the oxygen atoms of the sulfate ions. This enhances the SOFs of all the sulfate oxygen atoms to 1 to yield the formula

(15) Rothbauer, R.; Zigan, F.; O'Daniel, H. *Z. Kristallogr.* **1967**, *125*, 317.
(16) Fogg, A. M.; Green, V. M.; Harvey, H. G.; O'Hare, D. *Adv. Mater.* **1999**, *11*, 1466.
(17) Fogg, A. M.; Dunn, J. S.; Shyu, S.-G.; Cary, D. R.; O'Hare, D. *Chem. Mater.* **1998**, *10*, 351.
(18) Lei, L.; Millange, F.; Walton, R. I.; O'Hare, D. *J. Mater. Chem.* **2000**, *10*, 1881.
(19) Britto, S.; Thomas, G. S.; Kamath, P. V.; Kannan, S. *J. Phys. Chem. C* **2008**, *112*, 9510.
(20) Larson, A. C.; Von Dreele, R. B. *General Structure Analysis System* (*GSAS*); Los Alamos National Laboratory Report LAUR 86-748, 2004.
(21) Thomson, P.; Cox, D. E.; Hastings, J. B. *J. Appl. Crystallogr.* **1987**, *20*, 79.
(22) Treacy, M. M. J.; Deem, M. W.; Newsam, J. M. *DIFFaX*, Version 1.807.
(23) Treacy, M. M. J.; Newsam, J. M.; Deem, M. W. *Proc. R. Soc. London* **1991**, *A 433*, 499.
(24) Uvarova, Y.; Sokolova, E.; Hawthorne, F. C.; Karpenko, V. V.; Agakhanov, A. A.; Pautov, L. A. *Can. Mineral.* **2005**, *43*, 1511.

Table 1. Results of Wet Chemical Analysis and TGA Data

sample	Al/Zn ratio	A^{n-}/Zn ratio	% mass loss	approx. formula
ZA-1 LDH	2.8	0.63	32.2%	$[Zn_{0.218}Al_{0.612}(OH)_2][SO_4]_{0.136}\ 0.6H_2O$
Zn−Al−NO_3 LDH	2.96	1.2[a]	48.3%	$[Zn_{0.207}Al_{0.612}(OH)_2][NO_3]_{0.25}\ 0.74H_2O$
Zn−Al−CrO_4 LDH	2.96	0.40	43.7%	$[Zn_{0.207}Al_{0.612}(OH)_2][CrO_4]_{0.082}[NO_3]_{0.081}\ 0.85H_2O$

[a] The NO_3^- content in the LDH is calculated after accounting for Zn, Al, and water content.

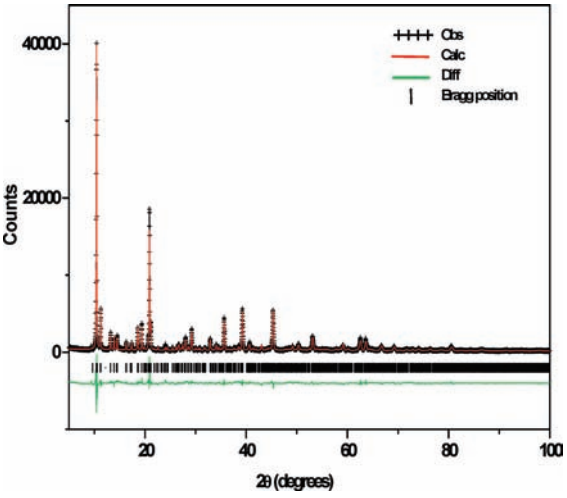

Figure 1. Final Rietveld fit of the observed PXRD profile of the ZA-1 LDH.

Table 2. Crystal Data and Structure Refinement Parameters of the ZA-1 LDH

crystal system	monoclinic
space group	$P2_1/n$
cell parameters/Å	a = 10.2853(5)
	b = 8.9057(4)
	c = 17.1200(5)
	β = 95.662(5)
volume/Å^3	1560.53(7)
data points	4778
parameters refined	80
no. of restraints	31
*R*wp	0.1362
*R*p	0.1054
reduced χ^2	11.45
$R(F^2)$	0.1066
*R*exp	0.042

$[(Zn_{0.5}\square_{0.5})(Al_{1.8}Zn_{0.1}\square_{0.1})(OH)_6)][SO_4]_{0.3}\cdot 1.8H_2O$ (see Table 1 for the experimentally determined empirical formula). This model gives an acceptable fit to the observed pattern as shown in Figure 1. The refinement conditions and atomic position parameters are given in Tables 2 and 3, respectively.

In Figure 2a is shown the IR spectrum of the sample ZA-1. In accordance with the IR spectra of LDHs,[25] broad bands are seen at ~3250 cm^{-1} due to hydrogen bonded OH stretching vibrations. However, in contrast to the brucite-based LDHs, a peak at ~3610 cm^{-1} is also seen pointing to the presence of non-hydrogen bonded hydroxyl groups. Vibrations due to the intercalated sulfate ion are seen at 1097 cm^{-1} corresponding to the ν_3 mode. Al−O−H bending vibrations are seen at 990 cm^{-1} and 930 cm^{-1}. The other vibrations of the SO_4^{2-} ions (ν_4) are presumably obscured by the lattice vibrations. Splitting of the ν_3 mode suggests a lowering of the symmetry of the SO_4^{2-} ion from the tetrahedral symmetry of the free sulfate. A Diamond[26] drawing of the structure is shown in Figure 2b. It can be seen that the sulfate ion is coordinated with one of its 2-fold axes parallel to the *b* crystallographic axis. The latter is also the defining 2-fold axis of the monoclinic crystal symmetry of nickelalumite. According to Halford,[27] for a "molecule in a crystal", the crystallographic axis is the principal axis of symmetry. The resultant symmetry of the sulfate ion in the nickelalumite structure is D_{2d}.[28] Below 600 cm^{-1} are seen a series of sharp peaks corresponding to Al−O and Zn−O lattice vibrations. The sharpness of the peaks is attributed to cation ordering.[25,11]

The TGA curve of sample ZA-1 is shown in Figure 3. The TGA curve indicates a three-step mass loss characteristic of a layered hydroxide. The first step (< 200 °C) is due to loss of intercalated and adsorbed water. The second step (200−600 °C) corresponds to dehydroxylation while the last step (> 650 °C) corresponds to volatilization of sulfate ions. In accordance with the elemental analysis data, the mass loss

Table 3. Refined Unit Cell and Atomic Parameters after the Final Cycle of Refinement[a]

atom type	Wyckoff position	*x*	*y*	*z*	SOF	U_{iso}/Å^2
Zn1	4*e*	0.7507(4)	0.5053(4)	0.4948(5)	1.0	0.00041
Zn2	4*e*	−0.0027(5)	0.3138(9)	0.5015(4)	0.224	0.00043
Al1	4*e*	−0.0027(5)	0.3138(9)	0.5015(4)	0.672	0.0205
Al2	4*e*	0.4976(8)	0.6732(9)	0.5039(3)	1.0	0.0030
Al3	4*e*	0.2523(1)	0.1615(2)	0.4906(8)	1.0	0.0082
Al4	4*e*	0.2475(6)	−0.1631(3)	0.4950(4)	1.0	0.00824
S1	4*e*	0.4904(5)	0.1125(9)	0.7402(7)	0.732	0.01707
O1	4*e*	0.5841(1)	0.4922(9)	0.5549(2)	1.0	0.005
O2	4*e*	0.9261(8)	0.4936(6)	0.4479(9)	1.0	0.005
O3	4*e*	0.6400(3)	0.3280(1)	0.4362(4)	1.0	0.005
O4	4*e*	0.8444(1)	0.3041(8)	0.5735(6)	1.0	0.005
O5	4*e*	0.1046(8)	0.1751(4)	0.5503(2)	1.0	0.005
O6	4*e*	0.1847(2)	0.0031(3)	0.4333(9)	1.0	0.005
O7	4*e*	0.6560(9)	0.6972(9)	0.4542(9)	1.0	0.005
O8	4*e*	0.8569(7)	0.6800(3)	0.5563(6)	1.0	0.005
O9	4*e*	−0.1150(2)	0.1771(4)	0.4317(4)	1.0	0.005
O10	4*e*	0.6104(24)	0.8027(29)	0.5761(14)	1.0	0.005
O11	4*e*	0.3947(22)	−0.1945(27)	0.4453(14)	1.0	0.005
O12	4*e*	0.3126(21)	0.0016(25)	0.5497(12)	1.0	0.005
O13	4*e*	0.5052(5)	0.0108(9)	0.6782(5)	1.0	0.01617
O14	4*e*	0.9240(7)	0.4705(2)	0.2925(5)	1.0	0.00908
O15	4*e*	0.6106(1)	0.1634(6)	0.7782(5)	1.0	0.00543
O16	4*e*	0.4135(2)	0.2436(1)	0.7248(7)	1.0	0.025
O17	4*e*	−0.1673(6)	−0.2212(6)	0.2142(9)	1.0	0.025
O18	4*e*	0.7248(3)	0.4268(4)	0.7251(6)	1.0	0.025
O19	4*e*	−0.0456(8)	−0.0141(4)	0.2929(4)	1.0	0.025

[a] a = 10.2853(5) Å, b = 8.9057(4) Å, c = 17.1200(5) Å, β = 95.662(5)°.

(25) Hernandez-Moreno, M. J.; Ulibarri, M. A.; Rendon, J. L.; Serna, C. *J. Phys. Chem. Miner*. **1985**, *12*, 34.

(26) *Diamond*, Version 2.0; Brandenburg, K., Putz, H.; Crystal Impact GbR: Bonn, Germany, 1998.

(27) Halford, R. S. *J. Chem. Phys*. **1946**, *14*, 8.

(28) Adler, H. H.; Kerr, P. F. *Am. Mineral*. **1965**, *50*, 132.

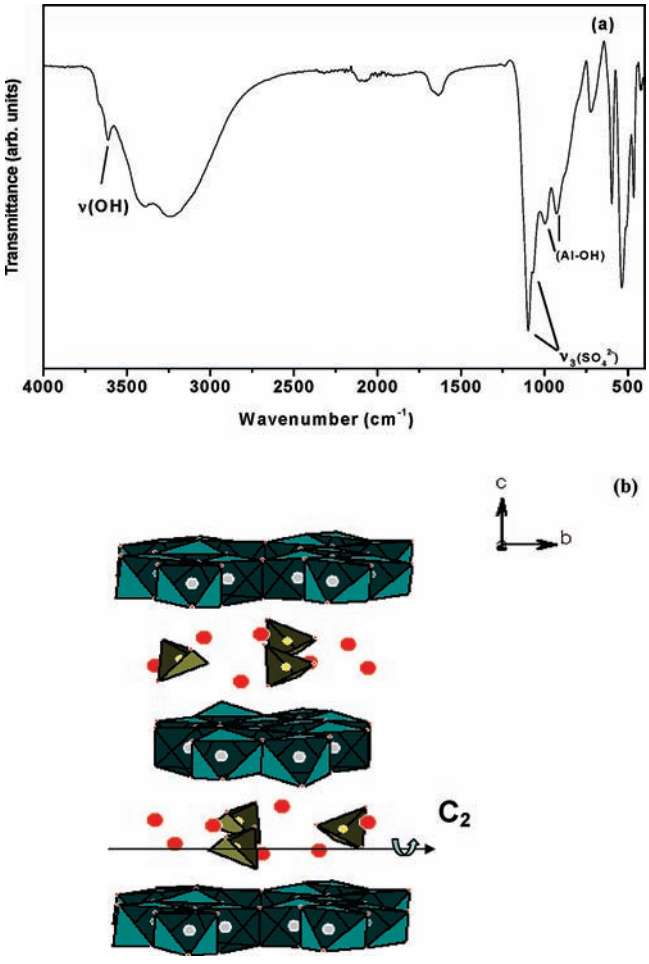

Figure 2. (a) IR spectrum of the ZA-1 LDH and (b) a model of the refined structure.

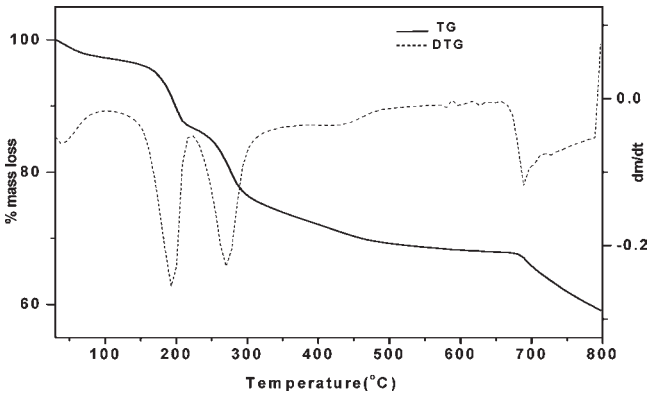

Figure 3. TGA-DTG plot of the ZA-1 LDH.

observed until 600 °C (Obs: 32.2%, Calc: 33.4%) is consistent with the following reaction:

$$[Zn_{0.204}Al_{0.612}(OH)_2][SO_4]_{0.122}\cdot 0.6H_2O \rightarrow 0.122ZnSO_4 + 0.306Al_2O_3 + 0.08ZnO$$

We now turn to the structure of the sample ZA-2 obtained by aging ZnO in $Al_2(SO_4)_3$ whose PXRD pattern (see Figure 4a) exhibits considerable broadening of peaks. The peaks can be indexed to a monoclinic cell (Table 4) from which it is evident that ZA-2 has a structure that is closely related to ZA-1

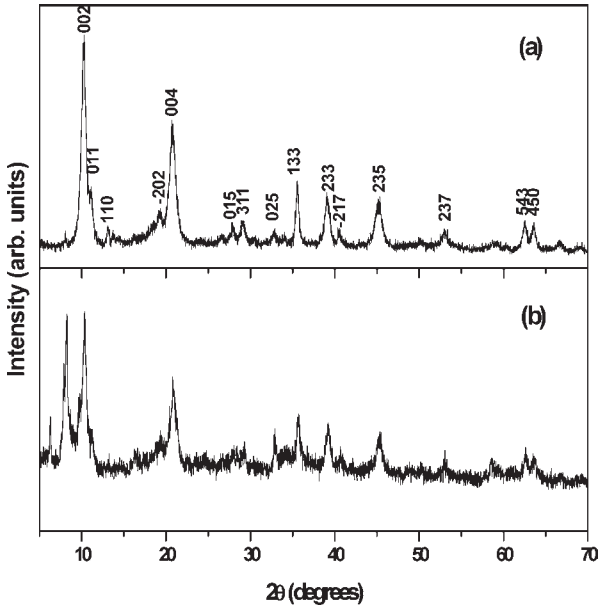

Figure 4. (a) PXRD pattern of the ZA-2 LDH, and (b) the same preparation with an additional 10.7 Å phase.

Table 4. Observed and Calculated *d* spacings of the Disordered ZA-2 LDH[a]

d (obs; Å)	*d* (calc; Å)	*hkl*
8.629	8.555	002
7.978	7.922	011
6.763	6.725	110
4.603	4.602	202
4.278	4.277	004
3.189	3.195	015
3.075	3.073	311
2.721	2.717	025
2.526	2.527	133
2.303	2.300	233
2.228	2.228	−217
2.005	2.006	235
1.726	1.727	237
1.486	1.486	−543
1.463	1.464	450

[a] a = 10.267 Å, b = 8.938 Å, c = 17.206 Å, β = 96.04°.

(See Supporting Information SI.4 for a comparison of the raw PXRD patterns of ZA-1 and ZA-2). The IR spectrum of ZA-2 (Figure 5a) is also similar to that of ZA-1. However, ZA-2 is sensitive to hydration and yields a phase with a larger interlayer distance (10.7 Å) (Figure 4b) which appears as an impurity in some preparations.

It is known that broadening of peaks in a PXRD pattern can be due to either crystallite size effects or structural disorders.[29−32] The effects of crystallite size (finite layer width and finite thickness) are shown in Supporting Information SI.5 and SI.6, respectively. It is clear that the XRD profiles obtained on limiting disk diameter does not give a visual match with the observed PXRD pattern. In the observed pattern, the three reflections in the mid-2θ region (35−50°) show a decrease in peak height with increase in angle. On the other hand, limiting disk diameter to just 200 nm results in an

(29) Delmas, C.; Tessier, C. *J. Electrochem. Soc.* **1997**, *7*, 1439.
(30) Tessier, C.; Haumesser, P. H.; Bernard, P.; Delmas, C. *J. Electrochem. Soc.* **1999**, *146*, 2059.
(31) Ramesh, T. N.; Jayashree, R. S.; Kamath, P. V. *Clays Clay Miner.* **2003**, *51*, 570.
(32) Viani, A.; Gualtieri, A. F.; Artioli, G. *Am. Mineral.* **2002**, *87*, 966.

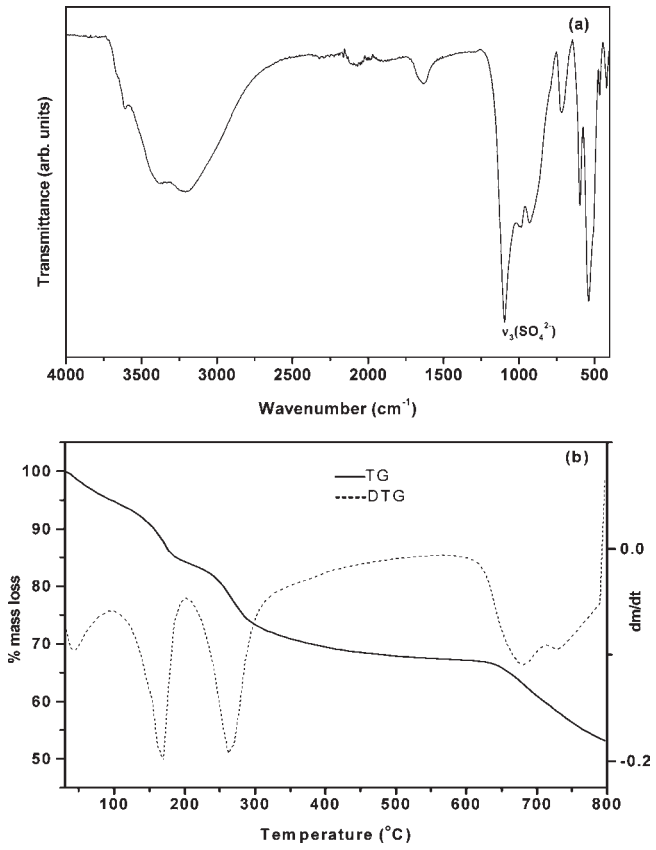

Figure 5. (a) IR spectrum and (b) TGA-DTG plot of the ZA-2 LDH.

increase in peak height with increasing angle. In addition there is an increase in the peak height of the 011 reflection with a decrease in the disk diameter. This is not seen in the observed pattern. The fwhm of the 002 reflection of the observed pattern (~0.6°) is obtained on limiting the crystallite thickness to 20 layers. However, limiting crystallite thickness results in a mismatch of the intensities of other reflections. Therefore crystallite size effects are inadequate to explain the observed broadening of lines in the PXRD pattern.

In layered materials, structural disorder can arise because of the following: (a) interstratification, (b) stacking faults, or (c) turbostraticity. The TGA data shown in Figure 5b indicates a higher water content (15.6%) in ZA-2 compared with that in the ordered sample ZA-1 (12.6%). Therefore we first simulate the effect of hydration on the PXRD pattern of nickelalumite by the random inclusion of excess water molecules in the interlayer region. This is done by the interstratification of nickelalumite with the hydrated phase of *d*-spacing, 10.7 Å. The results are given in Supporting Information SI.7. On increasing interstratification, the intensity of the 002 reflection progressively diminishes relative to the 011. The observed pattern comprises an intense 002 reflection and a weak 011 reflection. This mismatch shows that interstratification is inadequate to explain the observed PXRD profile of ZA-2.

Structural disorder due to stacking faults is particularly ubiquitous in layered materials because of the anisotropy in bonding that is a characteristic feature of these materials. As a result of the weak bonding between adjacent layers, the layers may stack one above the other in a number of equivalent ways to give rise to different polytypes. In cases where differences in energy between the various polytypes are small, it is rare to find pure polytypes of a material and instead random intergrowths of two or more energetically equivalent polytypes occur giving rise to materials with stacking disorders whose local structure matches that of one of the polytypes. Stacking faults are crystallochemically more likely than a completely random orientation of adjacent layers (turbostraticity) wherein interatomic distances are unlikely to be conserved.

The principles of Order−Disorder Theory (OD Theory)[33−35] are used to work out the possible polytypes of the structure. For a particular type of layer, there may be an infinite number of ways by which adjacent layers may be stacked relative to each other giving rise to an infinite number of possible stacking sequences. However, only those stacking sequences that conserve the symmetry elements of the single layer are considered as likely polytypes. We therefore first look at the symmetry elements present in a single layer and then at the symmetry relationships between adjacent layers of nickelalumite.

A single layer of nickelalumite has the following symmetry elements:

(a) mirror plane perpendicular to b at $b/2$
(b) 2-fold axis along b at $a/2$.

Two adjacent layers of the structure of nickelalumite are related by the following symmetry elements:

(a) n-glide planes perpendicular to b at $b/4$ and $3b/4$ with translational components $a/2 + c/2$.
(b) 2-fold screw axis 2_1 parallel to the layer plane along b at $a/2$.

Possible polytypes may be derived from the knowledge of the symmetry of the single layer and the symmetry relationships between two adjacent layers by making use of the following criterion:

The possible symmetry operations relating adjacent layers may differ from those present in a single layer only in their translational components.

Therefore possible polytypes are those in which the 2-fold axis is retained along b but the translational component of the screw is either 1 or 1/2.

In Figure 6a and Figure 6b is shown a DIFFaX simulation of the polytypes obtained by assuming that the 2-fold axis along b has a translational component of $b/2$ and b respectively. The pattern in Figure 6a corresponds to the polytype with a 2_1 screw axis which generates the structure of nickelalumite. We call this the $2M_1$ polytype. The pattern in Figure 6b corresponds to a possible new polytype with 2-fold axis along b in which the vacancies are ordered down the c-axis. We call this the $2M_2$ polytype.

A comparison of the two DIFFaX simulations shows that in the new polytype, the $00l$ and $h0l$ reflections remain unaffected. It can be seen that the main difference between the two polytypes is in the hkl ($k \neq 0$) reflections. In the $2M_1$ polytype, reflections with l odd are more intense than l even whereas, in the $2M_2$ polytype reflections with l even are more intense that l odd. Thereby $2M_1$ is characterized by an intense 011 reflection and $2M_2$ by an intense 010 reflection.

(33) Dornberger-Schiff, K. *Acta Crystallogr.* **1956**, *9*, 593.
(34) Dornberger-Schiff, K.; Grell-Niemann, H. *Acta Crystallogr.* **1961**, *14*, 167.
(35) Dornberger-Schiff, K. *Acta Crystallogr.* **1982**, *A38*, 483.

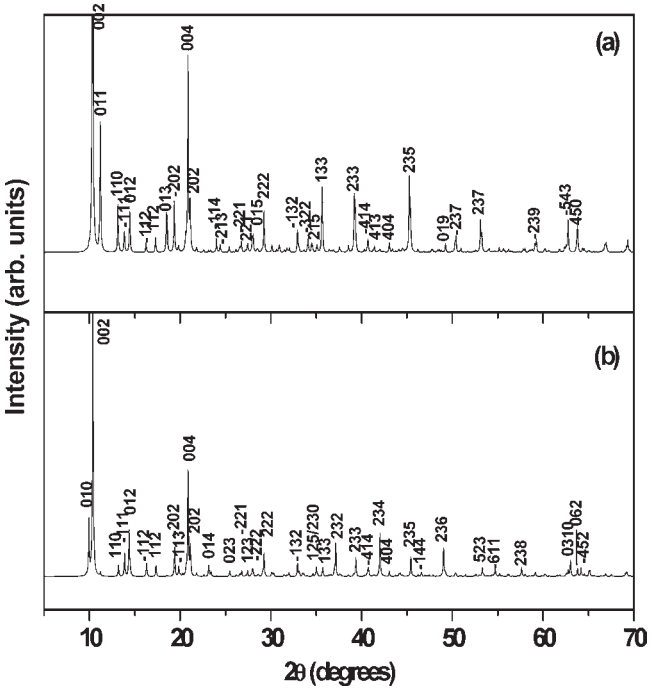

Figure 6. DIFFaX simulated PXRD patterns expected of the (a) $2M_1$ polytype corresponding to the nickelalumite structure and (b) the hypothetical $2M_2$ polytype.

In Figure 7a is shown the DIFFaX simulation of the $2M_1$ polytype with different degrees of stacking faults of the $2M_2$ type. It can be clearly seen that incorporation of these faults results in a lowering of the intensity of the 011 reflection. It can be seen that in the experimental pattern also the intensity of the 011 reflection is lowered compared to that in the ordered crystal.

In Figure 7b is shown the DIFFaX simulation of the $2M_1$ polytype containing 10% interstratification and 15% of stacking faults of the $2M_2$ type. It can be seen that this gives a reasonable fit to the experimental pattern ($R_p = 0.176$).

The following question arises out of the observations made above:

Why does the preparation using bayerite as a precursor result in a highly crystalline product whereas synthesis by reaction of ZnO with $Al_2(SO_4)_3$ results in a disordered compound.

A comparison of the structures of nickelalumite and bayerite shows that a close structural relationship exists between the two. While nickelalumite has the cell parameters $a = 10.256$ Å, $b = 8.8815$ Å, $c = 17.099$ Å, $\beta = 95.54°$, bayerite has the cell parameters $a = 5.062$ Å, $b = 8.671$ Å, $c = 4.713$ Å, $\beta = 90.27°$. Figlarz et al. in their seminal work on "Topotaxy, Nucleation and Growth"[36] had defined a topotactic reaction as one in which "one crystalline phase is converted to the other with a definite and reproducible crystallographic relationship between the two and carries no implications regarding the reaction mechanism". By this definition the transformation of bayerite to LDH can be called a topotactic reaction ($a_{LDH} \sim 2 \times a_{bay}$, $b_{LDH} \sim b_{bay}$, $c_{LDH} \sim 4 \times c_{bay}$). Now whether the reaction proceeds through a topochemical pathway or not is difficult to ascertain by experimental methods. There are two possible mechanisms by which the reaction could occur:

(a) by topotactic imbibition of the cation through the triangular faces of the $\square(OH)_6$ octahedra as has been proposed for the formation of the Li−Al LDHs.
(b) by dissolution-reprecipitation.

Two factors are said to affect the incorporation of a cation into the voids of $Al(OH)_3$: the size of the cation and its enthalpy of hydration. Li^+ with an ionic radius of 0.9 Å is larger than the divalent cations and yet can be incorporated into $Al(OH)_3$. The enthalpy of hydration therefore is the predominant factor governing cation imbibition into $Al(OH)_3$. Li^+ has a much lower enthalpy of hydration (-515 kJ mol^{-1}) compared to the divalent cations such as Mg^{2+}(-1922 kJ mol^{-1}), Ni^{2+}(-2106 kJ mol^{-1}), Co^{2+}(-2054 kJ mol^{-1}), or Zn^{2+}(-2044 kJ mol^{-1}).[37] It is therefore unlikely that Al-rich LDHs containing divalent cations can be formed through a topotactic imbibition process.

A closer look at the structure of the Al-rich II−III LDH shows that in the ordered sample, ZA-1, while the cations and vacancies are ordered along the *a*-*b* plane in a regular fashion, translation of adjacent layers by $b/2$ implies that there is no ordering of vacancies or Zn^{2+} ions down the *c*-axis. This confers on the structure a degree of charge delocalization that is reflected in the extensive hydrogen bonding between the intercalated species whereby hydrogen bonding between sulfate ions and interlayer water molecules is greater than between sulfate and layer hydroxyl groups. This is also reflected in the presence of vibrations due to non-H bonded hydroxyl groups in the IR spectrum. It is likely that the synthesis of Al-rich LDH prepared from bayerite takes place through a dissolution-reprecipitation mechanism occurring at the solid-solution interface of bayerite. The slow kinetics of dissolution of bayerite at the solid-solution interface is responsible for the highly crystalline product obtained from the bayerite precursor. The disordered sample, ZA-2, on the other hand is formed by rapid dissolution of ZnO and precipitation of the LDH with the inclusion of stacking faults and interstratification.

Hydrothermal treatment of bayerite in solutions of $CoSO_4$ and $NiSO_4$ did not yield LDHs.

Anion Exchange Reactions. One of the major applications of LDHs is in anion exchange reactions. In general, univalent anions are more exchangeable than divalent ions. Therefore, nitrate containing bayerite-based LDHs were obtained by the use of $M(NO_3)_2$ (M = Co, Ni, Zn). The good match of the POWDERCELL[38] simulation of the nickelalumite PXRD pattern with the observed patterns of the nitrate-LDHs (Figure 8) shows that the nitrate LDHs (M = Zn, Co) also crystallize in the bayerite-based structure. The poor match in the intensities of the reflections between 10 and 20° 2θ is due to differences in the positions of nitrate when compared to the sulfate positions of the model structure.[14] The product from $Ni(NO_3)_2$ yielded a pattern which could not be unambiguously indexed to an bayerite-based LDH (data not shown).

The IR spectrum of Zn−Al−NO_3 LDH is shown in Supporting Information, SI.8. Splitting of the ν_3 vibration

(36) Figlarz, M.; Gerand, B.; Delahaye-Vidal, A.; Dumont, B.; Harb, F.; Coucou, A.; Fievet, F. *Solid State Ionics* **1990**, *43*, 143.

(37) Wulfsberg, G. *Inorganic Chemistry* 1st Indian ed.; University Science Books: Herndon, VA, 2002.

(38) Kraus, W.; Nolze, G. *POWDERCELL*, v. 2.4; Federal Institute for Materials Research and Training: Berlin, Germany, 2000.

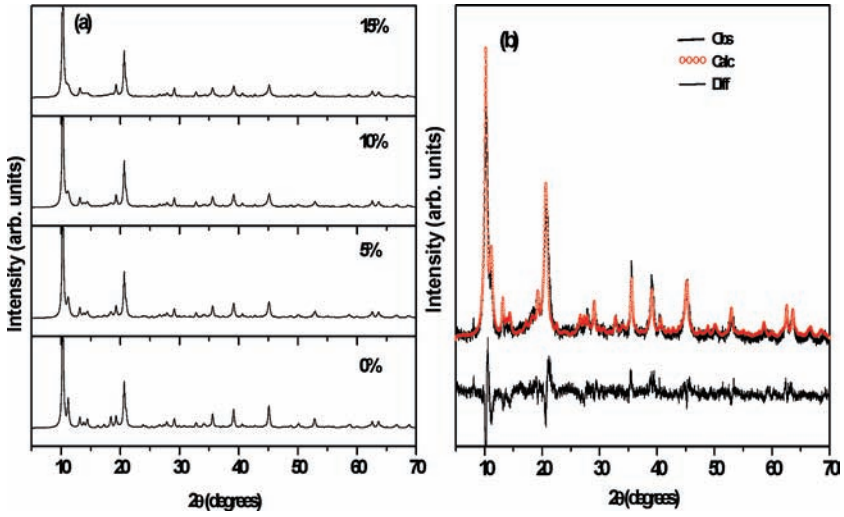

Figure 7. (a) DIFFaX simulated PXRD patterns of the $2M_1$ polytype incorporating different proportions of planar faults corresponding to the stacking motif of the $2M_2$ polytype and (b) a comparison of the observed PXRD pattern of the ZA-2 LDH with the DIFFaX simulated pattern of the $2M_1$ polytype containing stacking faults of the $2M_2$ polytype.

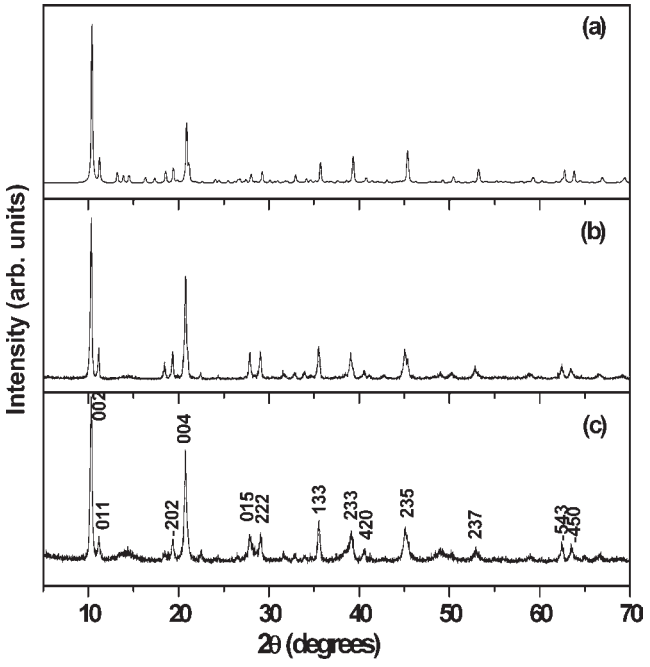

Figure 8. (a) POWDERCELL simulation of the nickelalumite structure compared with the PXRD pattern of the bayerite-based (b) Zn−Al−NO_3 LDH and the (c) Co−Al−NO_3 LDH.

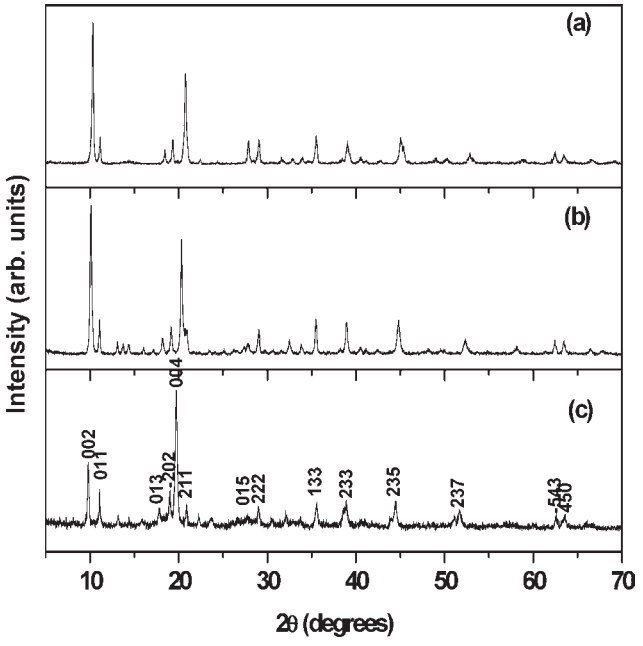

Figure 9. PXRD pattern of the (a) bayerite-based Zn−Al−NO_3 LDH and the products obtained after exchange of NO_3 for (b) CrO_4^{2-} and (c) MoO_4^{2-}.

of NO_3^- (1364 cm^{-1} and 1400 cm^{-1}) indicates a lowering of the symmetry of the NO_3^- ion from D_{3h} to C_{2v}.

The NO_3^- in the Zn−Al−NO_3 LDH could be exchanged for chromate and molybdate ions (Figure 9, Table 1). The IR spectrum of the chromate exchanged product is shown in Supporting Information, SI.9a, where the ν_3 vibration of the intercalated chromate ion is seen at ~860 cm^{-1}. Peaks due to residual nitrate can still be seen. In the case of exchange with molybdate ion, the exchange was carried out at pH 4.5. At this pH, the predominant molybdate species in solution is the $Mo_7O_{24}^{6-}$ ion. However the *d*-spacing of 8.9 Å points to intercalation of the tetrahedral MoO_4^{2-} species. The IR spectrum confirms (Supporting Information, SI.9b) this with the antisymmetric stretching vibration (ν_3) of the MoO_4^{2-} ion being observed at 813 cm^{-1}.

We also carried out anion exchange reactions of the NO_3-LDH with Cl^- and CO_3^{2-} (Supporting Information, SI.10). A shift in the *d*-spacing from 8.6 Å in the precursor to 7.5 Å in the products indicates that exchange has occurred. Both the products contain $Al(OH)_3$ (18.5° and 20.4° 2θ) showing that the precursor has decomposed during anion exchange.

It is clear from the above observations that the bayerite-based LDHs have distinctly different anion exchange characteristics when compared to the brucite-based II−III LDHs. O'Hare and co-workers[39] have shown that these LDHs exhibit shape selective intercalation properties but of equal significance is the anion exchange behavior with simple

(39) Williams, G. R.; Dunbar, T. G.; Beer, A. J.; Fogg, A. M.; O'Hare, D. *J. Mater. Chem.* **2006**, *16*, 1231.

anions. Among the brucite-derived II−III LDHs, it has been shown that the affinity of the LDH for a particular anion is governed primarily by hydrogen bonding and Coulombic interactions. The affinity of the brucite derived LDH for different anions varies in the order $CO_3^{2-} > SO_4^{2-} > Cl^- > NO_3^- \gg I^-$. Coulombic interactions dictate that the LDH has a stronger affinity for the divalent anions when compared to the monovalent ions. However, among the divalent anions, the greater affinity for CO_3^{2-} compared to SO_4^{2-} stems out of optimum hydrogen bonding arising out of a matching of the symmetry of the CO_3^{2-} with the trigonal prismatic sites available in the interlayer region. This high affinity for CO_3^{2-} sometimes poses a problem when carbonate free LDHs are required. The bayerite-derived Al-rich LDHs reported here on the other hand have a poor affinity for the CO_3^{2-} and Cl^- ions and a strong affinity for tetrahedral (SO_4^{2-}, MoO_4^{2-} and CrO_4^{2-}) ions and NO_3^- as reflected by the high crystallinity of the LDHs containing these ions. In these LDHs, cation ordering causes a lowering of the symmetry of the LDH to monoclinic ($P2_1/n$) and consequently the interlayer site symmetry is no longer purely octahedral or prismatic. Therefore unlike in the brucite-derived LDHs, in these LDHs there is no match between the molecular symmetry of the carbonate with the interlayer site symmetry. The preference for tetrahedral ions is to be expected on the basis of Halford's rules, whereby the 2-fold axis of the ion coincides with the 2-fold axis of the crystal. Another factor determining the affinity for a particular anion has been explained by Uvarova and co-workers,[24] on the basis of bond valence principles, to arise from a need to match the Lewis acidity of the sheets with the Lewis basicity of the interlayer ion. On the basis of this argument, the basicity of carbonate would be incompatible with the acidity of the sheets.

In conclusion, we see that the structure (including polytypism and structural disorder) as well as interlayer chemistry of the divalent ion containing Al-rich LDHs derived from bayerite are distinctly different from their brucite-based counterparts. This significantly adds to the versatility of the LDHs and contributes to a much wider range of properties and possible applications.

Acknowledgment. The authors thank the Department of Science and Technology (DST), Government of India for financial support. P.V.K. is a recipient of the Ramanna Fellowship of the DST. S.B. thanks the University Grants Commission for the award of a Senior Research Fellowship (NET).

Supporting Information Available: Further details are given in sections SI.1−SI.10 in the form of tables and figures. This material is available free of charge via the Internet at http://pubs.acs.org.